Analytical Mechanics of Chemical Reactions. VI. Rotational and Vibrational Distributions of the $H+H_2$ Reaction in a Plane*

SHIOU-FU WU AND R. A. MARCUS

Noyes Chemical Laboratory, University of Illinois, Urbana, Illinois 61801

(Received 16 August 1971)

Rotational and vibrational distributions for the exchange reaction $H+H_2 \rightarrow H_2+H$ are obtained numerically for reaction in a plane and compared with the vibrationally adiabatic solutions. Evidence is obtained regarding the two adiabatic solutions for the final rotational state predicted earlier and for the disappearance of one of these at higher initial relative velocity. Good agreement between calculations based on natural collision coordinates and these based on Cartesian coordinates was found, where tested. The vibrational motion for reaction in a plane is fairly adiabatic on the average at energies of thermal interest. Connections with other properties are noted. The results support the idea of statistical adiabaticity suggested earlier in this series and thus support a derivation of activated complex theory based on this concept.

I. INTRODUCTION

Certain vibrational–rotational states, which we have termed "vibrationally adiabatic" (VA),[1] have been discussed in earlier papers of this series[2–6] relating activated complex theory to molecular dynamics for the bimolecular reaction

$$A+BC \rightarrow AB+C. \tag{1.1}$$

To describe such states in a quantitative way along the reaction coordinate, a curvilinear set of coordinates may be introduced ("natural collision coordinates")[2,4] having the property that during the collision the new coordinates pass smoothly from those suited to reactants to those suited to the activated complex and then to those suited to products.

A sufficient condition for activated complex theory to follow from the dynamics is that the reaction be vibrationally adiabatic (VA) from the reactants' region of configuration space to that of the activated complex.[6–8] A weaker and more realistic condition is that it be statistically adiabatic,[3,5] i.e., VA when averaged over initial vibrational and rotational phases, at least in *either* of two regions: from reactants to activated complex or from activated complex to products.[9]

In Paper V we tested quantitatively some of these ideas (vibrational adiabaticity, statistical adiabaticity and nonadiabaticity) for the case of linear reactive collisions, by comparing exact (numerical) and analytical classical mechanical results for vibrational energy changes and other properties.[10] Encouraging agreement between these results for the $H+H_2 \rightarrow H_2+H$ reaction was obtained. In earlier papers[2] and in this comparison[6] we distinguished VA which takes into account curvilinear contributions ("curvilinear VA"), and VA which does not ("rectilinear VA"). The cited agreement refers to the former.

In the present paper we consider some numerical tests for reaction in a plane, using the theoretical formalism described in Paper III and IV. An extension of a theory from linear to planar collisions represents an appreciable step in the direction toward realism, since rotations and orbital motions now become possible and their effect on the motion along the reaction coordinate can be investigated.

II. THEORY

The notion of VA, like the notion of adiabaticity in other systems, implies an adiabatic-correlation diagram describing the correlation of vibrational–rotational states of the reactant with those of activated complex and with those of product. In the case of linear collisions[2] in the three-center reaction (1.1), the nature of the adiabatic correlation was such that the vibrational quantum number of the activated complex A···B···C (a symmetric stretching) equalled that of BC.

To recall the adiabatic correlation described in Part IV for reaction in a plane, we first recall the nature of the natural collision coordinates defined earlier[4]: In the center-of-mass system of coordinates these coordinates are $(s, \rho, \varphi, \gamma)$. s is the reaction coordinate. ρ is a vibrational coordinate associated with the vibration of the reactant BC at large negative s, with a symmetric stretching of A···B···C for small s, i.e., in the activated complex region, and with the vibration of the product AB at large positive s. φ is an angle describing the orientation of the "body-fixed axes" of the system, and represents the orientation of the line of centers of the two reactants at large negative s, the orientation of the principal axis of A···B···C at small s, and the orientation of the line of centers of the two products at large positive s. γ is an angle coordinate, describing at large negative s the rotation of the reactant BC relative to the body-fixed axis, at small s the bending vibration of A···B···C, and at large positive s the rotation of the product AB relative to the body-fixed axis.

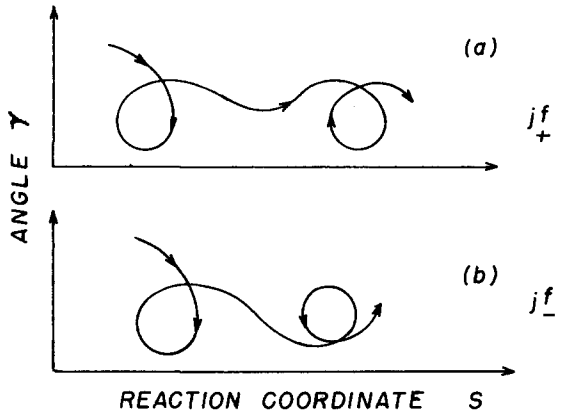

FIG. 1. Angular motion (natural collision coordinate γ) leading to the solutions j_+^f and j_-^f of Eqs. (2.9) and (2.10) of Figs. 1(a) and 1(b), respectively.

The rotational–vibrational wavefunctions at each value of s are functions of (ρ, γ, φ), and depend parametrically on s. The classical analogs of quantum numbers are the "action variables," J_ρ, J_φ, and J_γ. For example, J_ρ and J_φ are related to the vibrational quantum number v and total angular momentum quantum number J by

$$J_\rho = (v+\tfrac{1}{2})h, \qquad J_\varphi = Jh. \tag{2.1}$$

J_φ, like J, is thereby a constant of the motion. The adiabatic correlation for J_ρ is that

$$J_\rho = \text{const} \tag{2.2}$$

along the reaction coordinate.[4]

The nature of the adiabatic correlation for J_γ is more complicated.[5] First, the transition from a rotation of BC to a bending vibration of A···B···C is not necessarily a smooth one, since rotational motion is unidirectional and vibrational motion is bidirectional. Further, the correlation has to include the effect of the coupling between rotational and total angular momenta during the collision. It was shown that the bending–vibrational state of A···B···C correlating adiabatically with the initial rotational state of BC should be given by Eq. (A8) of Ref. 5:

$$J_\gamma{}^l = |\, J_\gamma{}^i - J_\varphi b \,|, \tag{2.3}$$

where $J_\gamma{}^l$, $J_\gamma{}^i$, and J_φ are the classical action variables

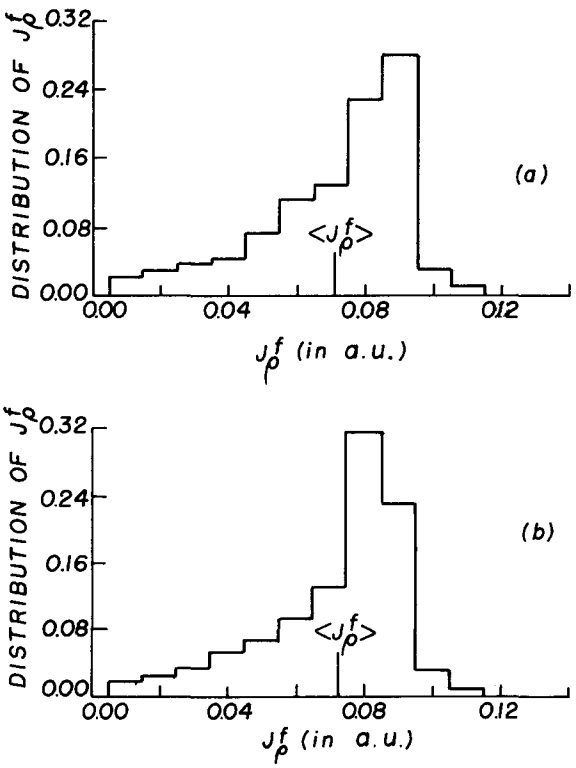

FIG. 2. Distribution of $J_\rho{}^f$ for $E_{tr}{}^i = 8.0$ kcal/mole: (a) $\sigma = 0.25$ a.u., $j^i = \pm 3.5\hbar$; $J_\rho{}^i = 0.0724$ a.u.; (b) $\sigma = 0.5$ a.u., $j^i = \pm 3.5\hbar$, $J_\rho{}^i = 0.0724$ a.u.

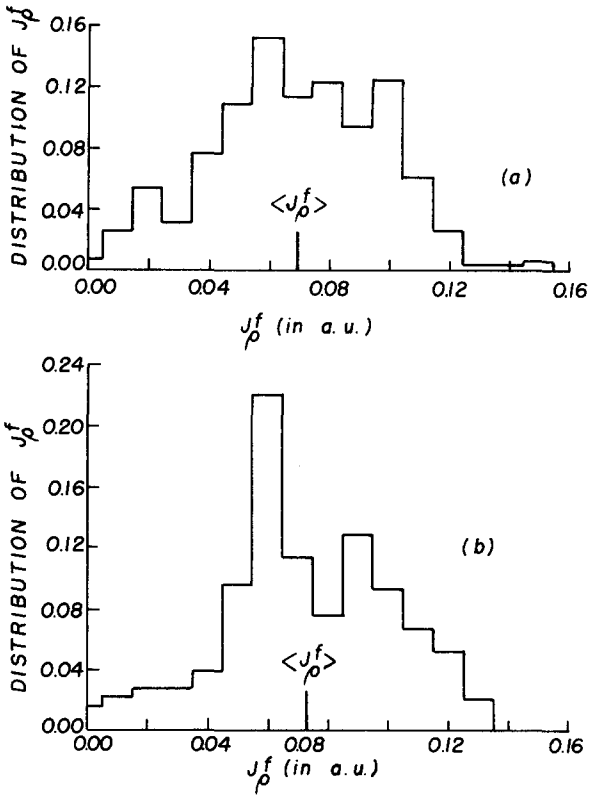

FIG. 3. Distribution of $J_\rho{}^f$ for $E_{tr}{}^i = 10.55$ kcal/mole and $\sigma = 1.0$ a.u.: (a) $j^i = \pm 1.4\hbar$, $J_\rho{}^i = 0.07525$ a.u.; (b) $j^i = \pm 3.5\hbar$, $J_\rho{}^i = 0.0724$ a.u.

TABLE I. Initial conditions, reactive range of initial rotational phase, and mean $\Delta J_\rho{}^f$ for $H+H_2 \rightarrow H_2+H$.

$E_{tr}{}^i$ (kcal/mole)	σ (a.u.)	l^i ($\hbar$)	j^i ($\hbar$)	$\Delta\Phi_{act}$ [a] ($\pm 5°$)	$\langle J_\rho{}^f\rangle - J_\rho{}^i$ (a.u.)	Fig. (J_ρ)	Fig. (j^f)
8.0	0.5	−2.8	3.5	10–40	−0.00991	2	7
8.0	0.5	−2.8	−3.5	100–150	0.00317	2	7
8.0	0.25	−1.4	3.5	0–50	−0.00338	2	8
8.0	0.25	−1.4	−3.5	110–160	0.00148	8	2
10.55	1.0	−6.4	−3.5	80–140	0.00678	3	9
10.55	1.0	−6.4	−1.4	−20–70	0.00264	3	9
10.55	0.5	−3.2	5.5	−80–10	−0.00587	4	10
10.55	0.5	−3.2	−5.5	140–230	0.02507	4	10
10.55	0.5	−3.2	3.5	0–70	−0.00010	4	11
10.55	0.5	−3.2	−3.5	70–160	0.00582	4	11
10.55	0.5	−3.2	1.4	70–160	−0.00262	···	12
10.55	0.25	−1.6	3.5	0–80	0.00283	···	···
10.55	0.25	−1.6	1.4	70–170	−0.00075	···	···
11.5	0.5	−3.4	1.4	70–160	···	···	12
14.5	1.0	−7.5	3.5	0–90	−0.00454	5	13
14.5	1.0	−7.5	−3.5	30–130	0.00366	5	13
14.5	1.0	−7.5	1.4	70–160	−0.00265	5	14
14.5	1.0	−7.5	−1.4	150–250	0.01622	5	14
14.5	0.5	−3.8	5.5	−50–50	0.01216	6	15
14.5	0.5	−3.8	−5.5	100–210	0.02477	6	15
14.5	0.5	−3.8	3.5	10–110	0.01118	6	16
14.5	0.5	−3.8	−3.5	40–150	0.00443	6	16
14.5	0.5	−3.8	1.4	70–180	···	···	17
14.5	0.25	−1.9	3.5	10–120	0.01106	···	···
14.5	0.25	−1.9	1.4	80 180	···	···	···
15.5	0.5	−3.9	3.5	10–120	···	···	···
15.5	0.5	−3.9	1.4	70–180	···	···	17

[a] $\Delta\Phi_{act}$ is the reactive range corresponding to the reaction path, $A+BC \rightarrow AC+B$; while $[\Delta\Phi_{act}+180°]$ is the reactive range corresponding to the reaction path, $A+BC \rightarrow AB+C$. The l^i's and j^i's have been rounded to the nearest $0.1\hbar$. The actual j^i's are $\pm 1.414\hbar$, $\pm 3.464\hbar$, and $\pm 5.472\hbar$.

associated with the bending vibration, the initial rotation, and the total angular momentum. A similar relation obtains in an analogous quantum treatment.[11] The quantity b, which is less than unity, describes a certain ratio of distances characterizing the value of the reaction coordinate where the motion changes from a rotation to a bending vibration (Appendix B).

If the adiabatic correlation from activated complex to products is also included, Eq. (2.3) and an analogous equation for passage from activated complex to products yield[5]

$$J_\gamma{}^f - J_\varphi b^f = \pm (J_\gamma{}^i - J_\varphi b^i), \tag{2.4}$$

where i and f refer to initial and final values and where b^i and b^f refer to the "b" for the transition of rotation of BC to bending of A···B···C and of bending of A···B···C to rotation of AB, respectively, in Reaction (1.1).

Recalling that the rotational angular momentum j of the diatomic species equalled $FJ_\gamma/2\pi$, where F was a function of position along the reaction coordinate and varying from -1 initially to $+1$ finally, we had[5]

$$J_\gamma{}^i = -2\pi j^i, \qquad J_\gamma{}^f = 2\pi j^f. \tag{2.5}$$

Thus, for the final rotational angular momentum there were two VA solutions designated as $j_+{}^f$ and $j_-{}^f$ and found from Eq. (2.4) to be

$$j_+{}^f = j^i + J(b^f + b^i), \tag{2.6}$$

$$j_-{}^f = -j^i + J(b^f - b^i). \tag{2.7}$$

These two solutions for j^f correspond physically to the motions indicated schematically in Figs. 1(a) and 1(b), respectively. (Actual computer-calculated trajectories for the relevant natural collision coordinate γ

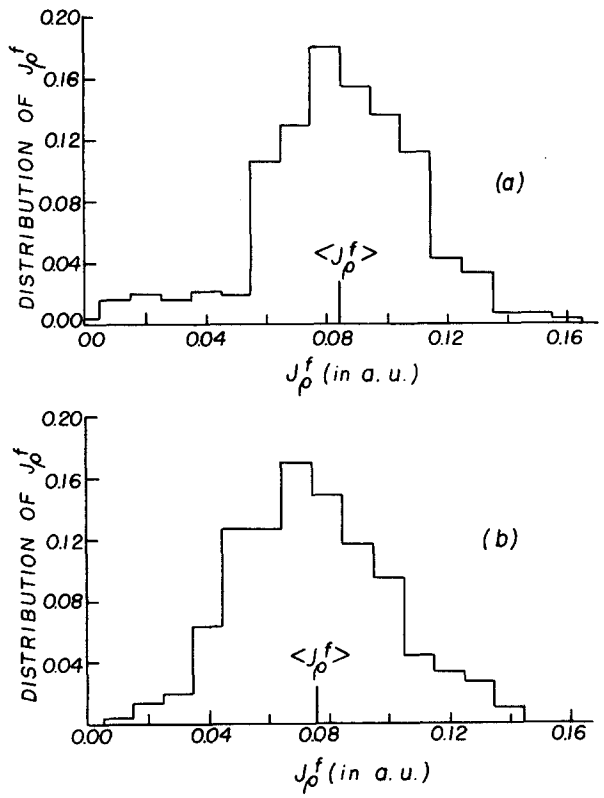

FIG. 4. Distribution of $J_\rho{}^f$ for $E_{tr}{}^i = 10.55$ kcal/mole and $\sigma = 0.5$ a.u.: (a) $j^i = \pm 5.5\hbar$, $J_\rho{}^i = 0.0721$ a.u.; (b) $j^i = \pm 3.5\hbar$, $J_\rho{}^i = 0.0724$ a.u.

are given later.) Equation (2.4) and hence Eqs. (2.6) and (2.7) presuppose a "rotation to bending vibration to rotation" transition. When the time spent by the system in the activated complex region is too small for the system to execute a bending vibration, e.g., when $E_{tr}{}^i$ is high, the solution $j_+{}^f$ in Fig. (1a) should disappear. The latter disappearance was not treated in Ref. 5.

When the reaction is symmetrical b^f equals $-b^i$ and will be denoted by b[5]:

$$b^f = -b^i = b \qquad \text{(symmetrical reaction)}. \quad (2.8)$$

Equations (6) and (7) then become[5]

$$\left.\begin{aligned} j_+{}^f &= j^i, && (2.9)\\ j_-{}^f &= -j^i + 2Jb \end{aligned}\right\} \text{ symmetrical reaction.} \quad (2.10)$$

A statistical adiabaticity will introduce a distribution of J_ρ and j^f about the VA values given in Eqs. (2.2), (2.9), and (2.10). Thus, for a given set of initial conditions, differing only in rotational and vibrational phase, the distribution of j^f will be bimodal, distributed about $j_+{}^f$ and $j_-{}^f$, but at high $E_{tr}{}^i$ it should become unimodal, distributed about $j_-{}^f$.

The $j_+{}^f$, given by (2.9), is independent of b. Only when J is low enough is $j_-{}^f$, given by (2.10), also b independent. For other J, b at first will be regarded as an unknown fixed parameter and then be compared

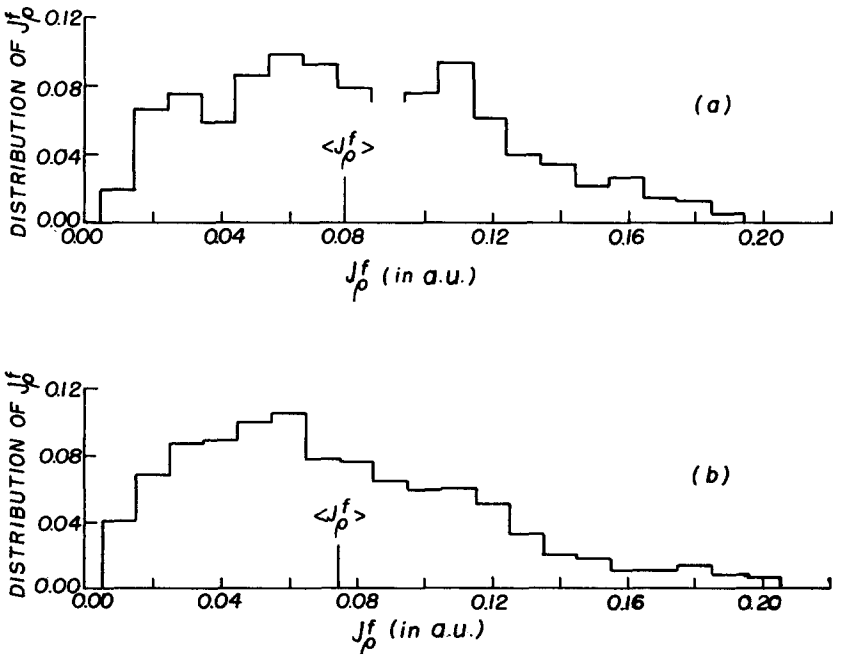

FIG. 5. Distribution of $J_\rho{}^f$ for $E_{tr}{}^i = 14.5$ kcal/mole and $\sigma = 1.0$ a.u.: (a) $j^i = \pm 1.4\hbar$, $J_\rho{}^i = 0.0725$ a.u.; (b) $j^i = \pm 3.5\hbar$, $J_\rho{}^i = 0.0724$ a.u.

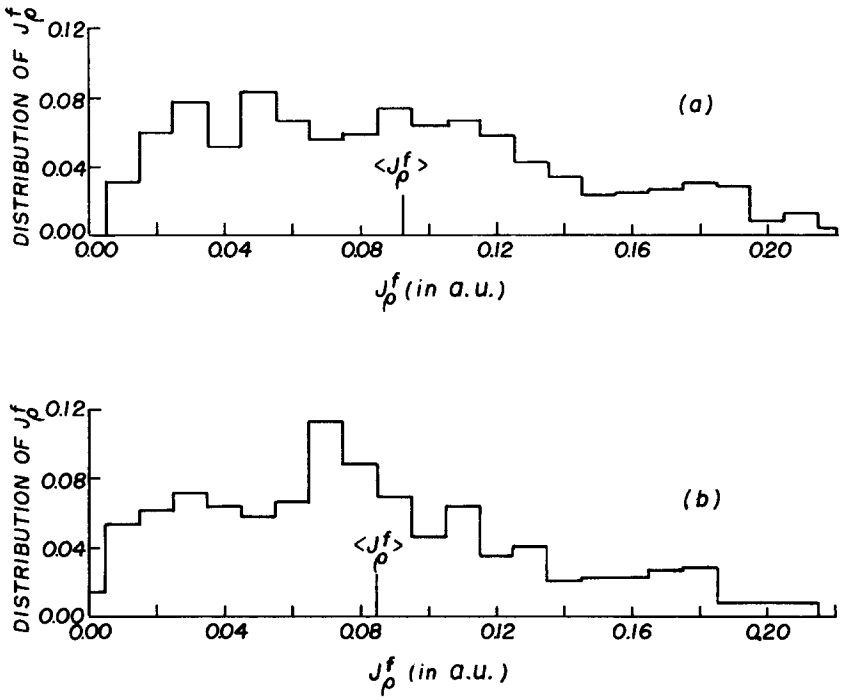

FIG. 6. Distribution of J_ρ^f for $E_{tr}^i = 14.5$ kcal/mole and $\sigma = 0.5$ a.u.: (a) $j^i = \pm 5.5\hbar$, $J_\rho^i = 0.0721$ a.u.; (b) $j^i = \pm 3.5\hbar$, $J_\rho^i = 0.0724$ a.u.

with an approximate *ab initio* calculation of b (Appendix B).

Child has developed a vibrationally adiabatic treatment which leads to (2.9) but not to (2.10),[8] i.e., leads to j_+^f but not to j_-^f. Arguments have just been given that j_+^f and j_-^f should both be important at low initial transitional energies, but that j_-^f should become more important at higher translational energies. The results in the next section bear on this aspect.

In any highly exothermic reaction where a sufficiently large internal translational energy occurs before the system passes into the "products' channel," one may expect, and one finds, considerable deviations from statistical adiabaticity (SA). In reactions such as $H+H_2$ there is a better chance for the fulfillment of SA provided the incident translational energy is not too high.

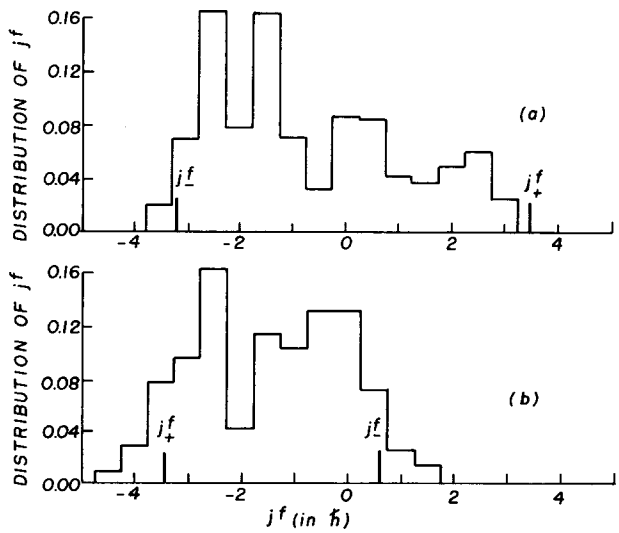

FIG. 7. Distribution of j^f for $E_{tr}^i = 8.0$ kcal/mole and $\sigma = 0.5$ a.u.: (a) $j^i = 3.5\hbar$, $J = 0.7\hbar$; (b) $j^i = -3.5\hbar$, $J = -6.3\hbar$.

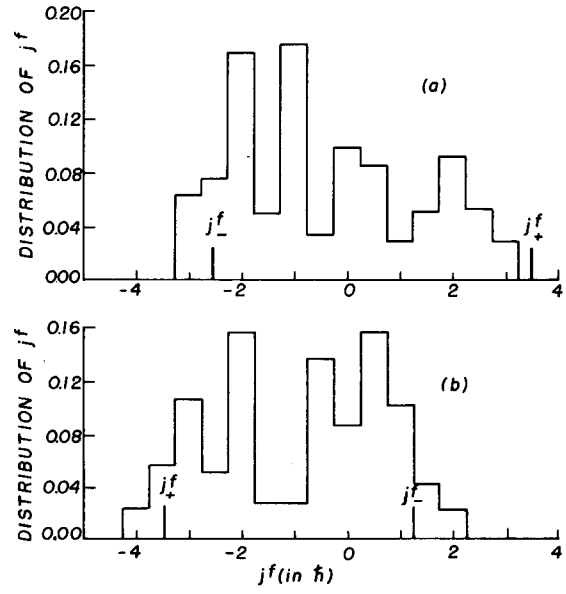

FIG. 8. Distribution of j^f for $E_{tr}^i = 8.0$ kcal/mole and $\sigma = 0.25$ a.u.: (a) $j^i = 3.5\hbar$, $J = 2.1\hbar$; (b) $j^i = -3.5\hbar$, $J = -4.9\hbar$.

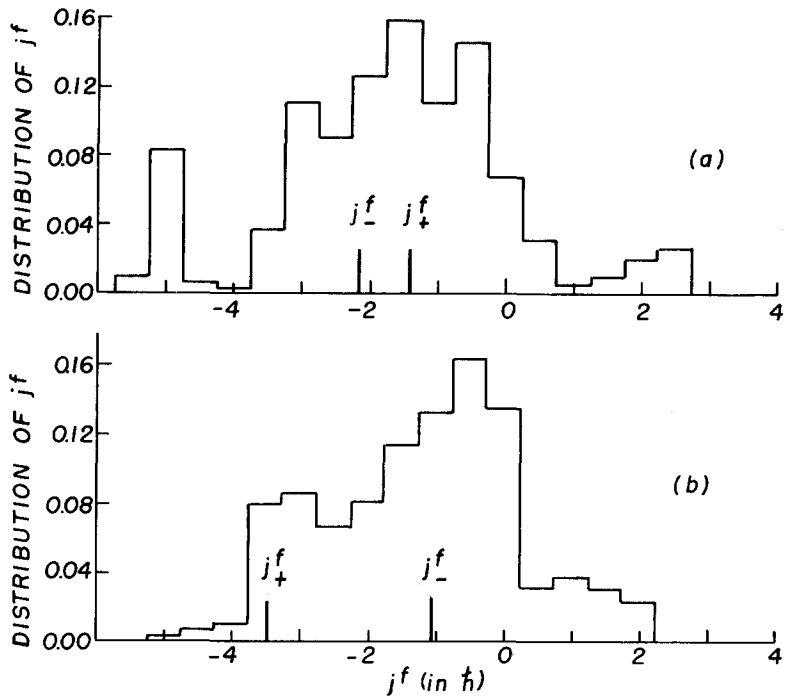

FIG. 9. Distribution of j^f for $E_{tr}{}^i = 10.55$ kcal/mole and $\sigma = 1.0$ a.u.: (a) $j^i = -1.4\hbar$, $J = -7.8\hbar$; (b) $j^i = -3.5\hbar$, $J = -9.9\hbar$.

III. PROCEDURE AND RESULTS

The classical mechanical equations of motion for the three-center reaction in a plane (four Cartesian coordinates in the center-of-mass system) were integrated numerically, using a fourth-order Runge–Kutta–Gill method.[12] Initial rotational and vibrational phases for BC were chosen at uniform intervals (Appendix A) to study the effect of initial phase on the dynamics. The initial constants of the motion for a BC molecule are not

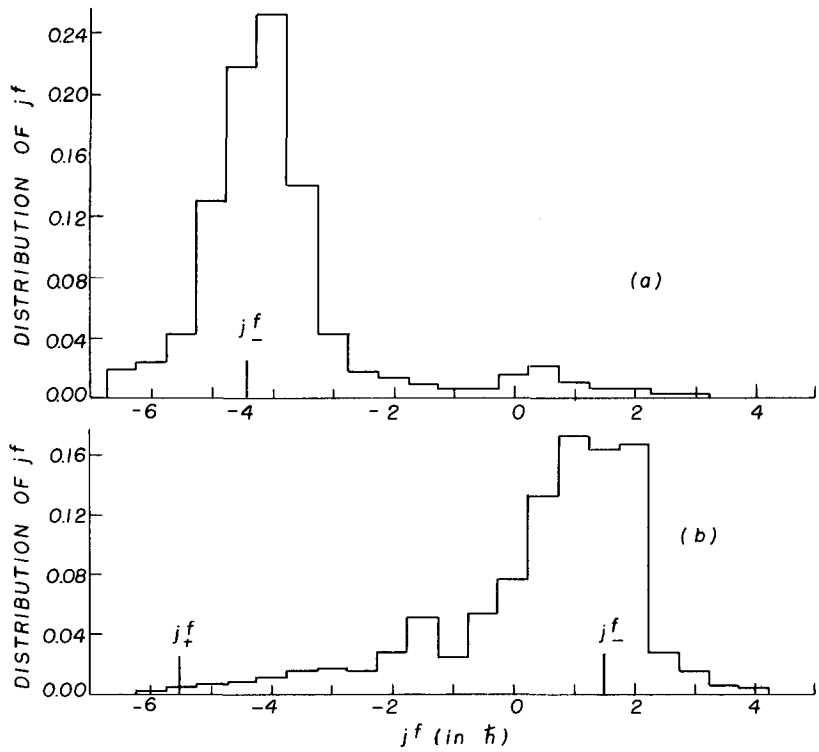

FIG. 10. Distribution of j^f for $E_{tr}{}^i = 10.55$ kcal/mole and $\sigma = 0.5$ a.u.: (a) $j^i = 5.5\hbar$, $J = 2.3\hbar$; (b) $j^i = -5.5\hbar$, $J = -8.7\hbar$. In Fig. 10(a), $j_+{}^f$ is $5.5\hbar$.

the rotational and vibrational energies, because of rotational–vibrational coupling. However, the action variables are initially constants. They include the rotational action $2\pi j$ and the vibrational action J_ρ (Appendix A).

The initial variables in the center-of-mass system are eight in number: four for BC [J_ρ, j, initial vibrational (δ) and rotational (Φ) phases (Appendix A)] and four for the relative motion of A and BC [the initial translational energy $E_{\rm tr}{}^i$ in the center of-mass, impact parameter σ, initial separation distance R, and direction of the initial relative translational velocity. The latter direction can be chosen to be along a fixed axis without loss of generality for the final values found for J_ρ and j.] The final values of J_ρ and j were calculated from the final Cartesian coordinates and momenta of the three atoms, as noted in Appendix A.

The reaction treated is

$$\mathrm{H}+\mathrm{H_2}\rightarrow\mathrm{H_2}+\mathrm{H}. \qquad (3.1)$$

As in Paper V the Porter–Karplus potential energy surface[13] for this reaction was used. The series of values used for $E_{\rm tr}{}^i$, σ, and j^i are summarized in Table I, the lowest $E_{\rm tr}{}^i$ being near the effective threshold energy for reaction. [The effective threshold energy in three-dimensional (3D) trajectory calculations[14] was 6.23, 7.08, and 7.16 kcal/mole for an angular momentum quantum number of 1, 3, and 5, respectively.] Initial rotational phases were chosen uniformly (every 10°–15°) over the reactive region of rotational phase; 24 initial uniformly chosen vibrational phases were used for each rotational phase. The reactive range of rotational phase $\Delta\Phi_{\rm act}$ for each set of values of $(E_{\rm tr}{}^i, \sigma, j^i)$ is also summarized in Table I. For the data in Table I the orbital angular momentum was negative for clockwise rotation of the line of centers; j^i was positive for counterclockwise rotation of BC. For each set of initial conditions there were two reactive ranges of initial rotational phase: $\Delta\Phi_{\rm act}$ and $\pi+\Delta\Phi_{\rm act}$ corresponding to the two reaction paths A+BC→AB+C and A+BC→AC+B, respectively.

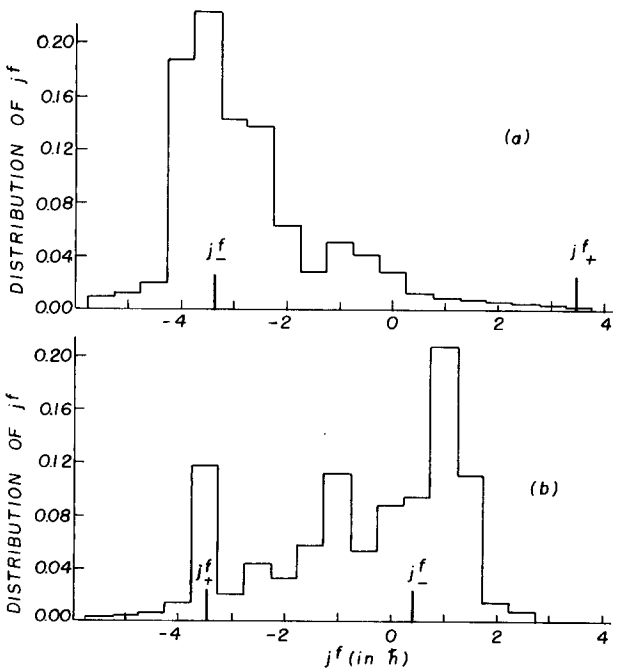

FIG. 11. Distribution of j^f for $E_{\rm tr}{}^i=10.55$ kcal/mole and $\sigma=0.5$ a.u.: (a) $j^i=3.5\hbar$, $J=0.3\hbar$; (b) $j^i=-3.5\hbar$, $J=-6.7\hbar$.

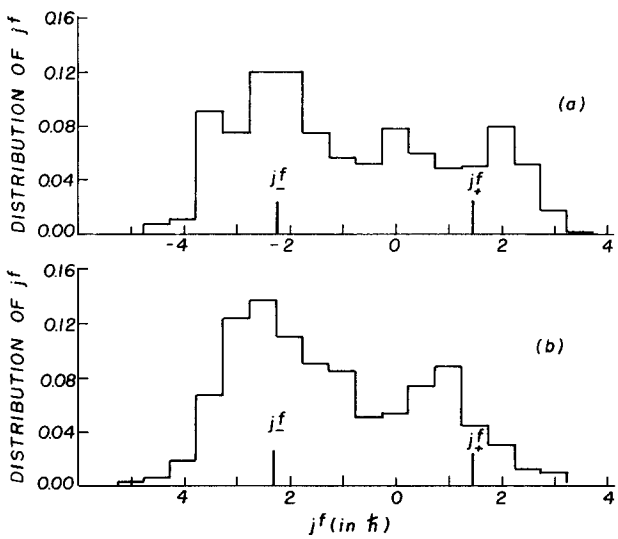

FIG. 12. Distribution of j^f for (a) $E_{\rm tr}{}^i=10.55$ kcal/mole, $\sigma=0.5$ a.u., $j^i=1.4\hbar$, $J=-1.8\hbar$; (b) $E_{\rm tr}{}^i=11.5$ kcal/mole, $\sigma=0.5$ a.u., $j^i=1.4\hbar$, $J=-1.9\hbar$.

In the present paper we concentrate on the distributions of j^f and $J_\rho{}^f$, rather than on the trajectories leading to those distributions. However, several results, in the form of plots of the dependence of j^f and $J_\rho{}^f$ on the initial phases, are given in Appendix C, since they illustrate the rotational–vibrational coupling and are also useful as a guide in semiclassical calculations.

Because of the uniform choice of initial vibrational and rotational phases the probability $P(j^f)\Delta j$ that the final rotational angular momentum of the diatomic product j^f lies in $(j^f-\frac{1}{2}\Delta j, j^f+\frac{1}{2}\Delta j)$ is

$$P(j^f)\Delta j=N^{-1}\sum_{\beta=1}^{N}\frac{\Delta\varphi_{\rm act}{}^\beta}{2\pi}, \qquad (3.2)$$

where N is the total number of reactive initial rotational phases β calculated, $\Delta\varphi_{\rm act}{}^\beta$ is the sum of reactive initial vibrational phases having the magnitude of j^f within $j^f\pm\frac{1}{2}\Delta j$ for the given specific initial rotational phase Φ_β. The step size Δj was $0.5\hbar$.

The distribution of final vibrational action $J_\rho{}^f$ was calculated from (3.2) with j^f replaced by $J_\rho{}^f$. The step

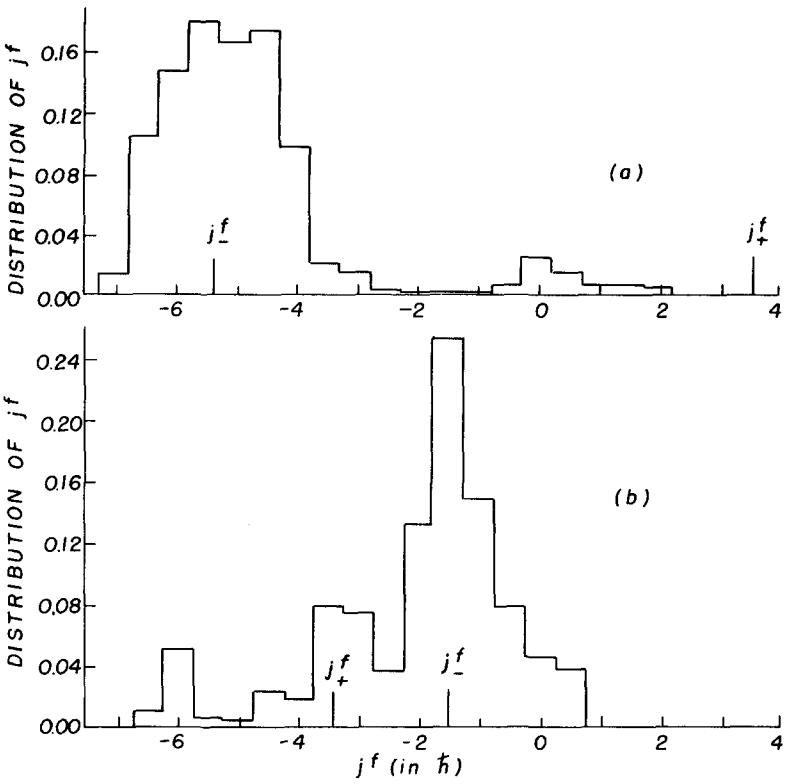

FIG. 13. Distribution of j^f for $E_{tr}{}^i = 14.5$ kcal/mole and $\sigma = 1.0$ a.u.: (a) $j^i = 3.5\hbar$, $J = -4.1\hbar$; (b) $j^i = -3.5\hbar$, $J = -11.0\hbar$.

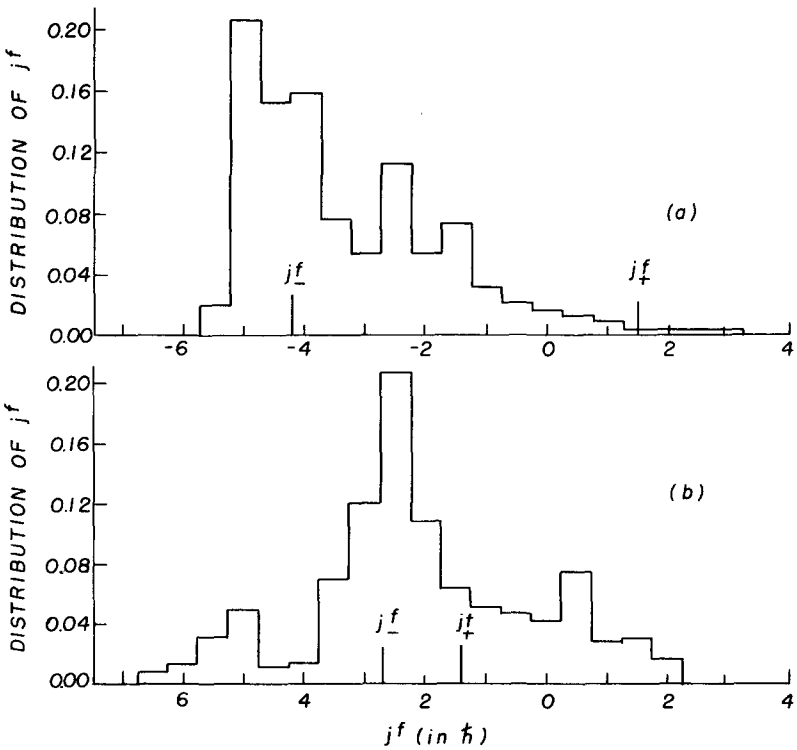

FIG. 14. Distribution of j^f for $E_{tr}{}^i = 14.5$ kcal/mole and $\sigma = 1.0$ a.u.: (a) $j^i = 1.4\hbar$, $J = -6.1\hbar$; (b) $j^i = -1.4\hbar$, $J = -8.9\hbar$.

size ΔJ_ρ was 0.02 a.u. The total distribution of $J_\rho{}^f$ contributed from both clockwise and counterclockwise rotation of the diatomic reactant is plotted in Figs. 2–6. Individual averages for the change of vibrational action, $\langle J_\rho{}^f\rangle - j_\rho{}^i$, for clockwise and counterclockwise j^i are listed in Table I.

The distribution of j^f for the clockwise and counterclockwise rotation of the diatomic reactant, each normalized to unity, is plotted in Figs. 7–17. The two vertical lines in these figures, labeled by $j_+{}^f$ and $j_-{}^f$, refer to the adiabatic values calculated from Eqs. (2.9) and (2.10), respectively, using for calculation of $j_-{}^f$ a single empirical value of $b=0.23$.

The total distribution of j^f contributed from both clockwise and counterclockwise rotation is the sum of the two sets of results, each weighted according to its reaction probability, using the reactive reaction probability range given in Table I. Since the latter is roughly the same for both clockwise and counterclockwise rotation, the total distribution of j^f in Figs. 7–17 is roughly equal to the sum of both sets of results.

The energy needed to reach the activated complex for a given $J_\gamma{}^l$, J_ρ, and J, can be termed the adiabatic threshold energy, $E_{\rm ad}{}^0(s^\ddagger)$. It is[15]

$$E_{\rm ad}{}^0(s^\ddagger) = V_1(s^\ddagger) + J_\gamma{}^l \nu_\gamma{}^\ddagger + E_v(s^\ddagger) + J^2\hbar^2/2\mu R^{\ddagger 2}, \quad (3.3)$$

where $V_1(s^\ddagger)$ is the potential energy at the saddle point, $J_\gamma{}^l$ is given by (B1), $\nu_\gamma{}^\ddagger$ is the frequency of bending vibration, $E_v(s^\ddagger)$ is the energy of symmetric stretching vibration, and $J\hbar$ is the total angular momentum. For an approximate calculation of the centrifugal potential $R^\ddagger$ was set equal to the distance from the origin to the saddle point.

The threshold values $E_{\rm ad}{}^0(s^\ddagger)$ were used to calculate the effective relative translational energy, $E_{\rm tr}{}^{\rm eff}$, as $E - E_{\rm ad}{}^0(s^\ddagger)$. The average change of vibrational action,

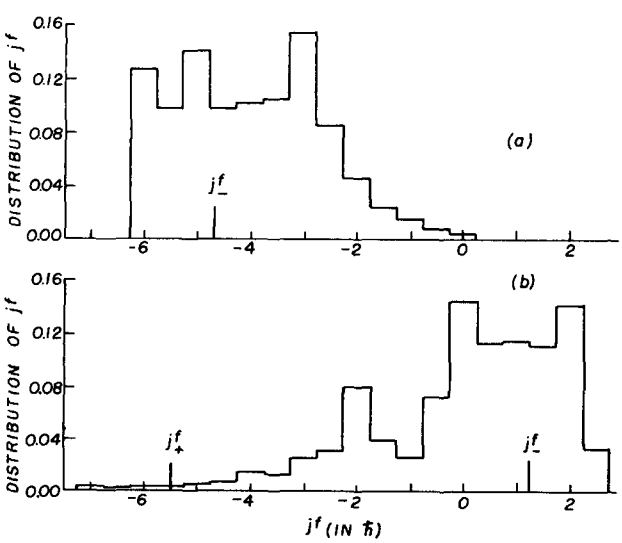

FIG. 15. Distribution of j^f for $E_{\rm tr}{}^i = 14.5$ kcal/mole and $\sigma = 0.5$ a.u.: (a) $j^i = 5.5\hbar$, $J = 1.7\hbar$; (b) $j^i = -5.5\hbar$, $J = -9.2\hbar$. In (a), $j_+{}^f$ is $5.5\hbar$.

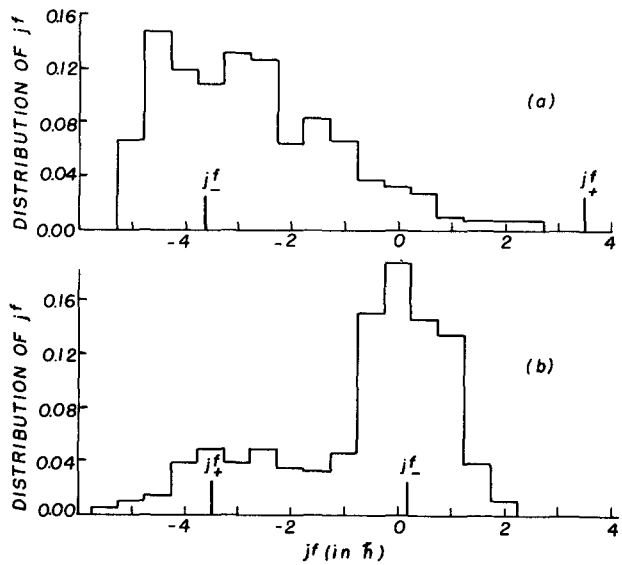

FIG. 16. Distribution of j^f for $E_{\rm tr}{}^i = 14.5$ kcal/mole and $\sigma = 0.5$ a.u.: (a) $j^i = 3.5\hbar$, $J = -0.3\hbar$; (b) $j^i = -3.5\hbar$, $J = -7.2\hbar$.

$\langle J_\rho{}^f\rangle - j_\rho{}^i$, is plotted vs $E_{\rm tr}{}^i$ and vs $E_{\rm tr}{}^{\rm eff}$ in Figs. 18 and 19, respectively.

To gain further insight into the results the exact equations of motion were expressed in terms of natural collision coordinates and integrated numerically. A plot of $\gamma(s)$ for several vibrational phases and two different rotational phases, at $E_{\rm tr}{}^i = 10.55$ kcal/mole, is given in Figs. 20 and 21. A comparison of data obtained with Cartesian coordinates with those obtained with natural collision coordinates is given in Fig. 22, where the dots refer to the latter (those at 1, 2, 3 being for $\Phi = 60°$ and those at 4, 5, 6 being for $\Phi = 20°$).

The activated complex had a mean ABC (or ACB) bond angle of 155° and a width at half-height of about 20°, for the range of initial conditions given in Table I.

IV. DISCUSSION

Data for reaction in a line, in a plane, and in space will be referred to as 1D, 2D, and 3D, following customary usage.

Several observations on the vibrational distributions are the following:

(1) In conjunction with Figs. 2-6 the 2D data in Figs. 18 and 19 show that statistical adiabaticity is fulfilled closely for $E_{\rm tr}{}^{\rm eff}$'s of interest in thermal studies of this reaction (a few kcal/mole). The 1D results are given for comparison in Figs. 18 and 19.

(2) Deviations from vibrational adiabaticity are reflected by there being a spread of values of $J_\rho{}^f$ in Figs. 2–6 instead of a single value. Thus, it is encouraging that the concept of statistical adiabaticity seems satisfactory. Deviations from vibrational adiabaticity were treated analytically in earlier papers of this series.[2,10]

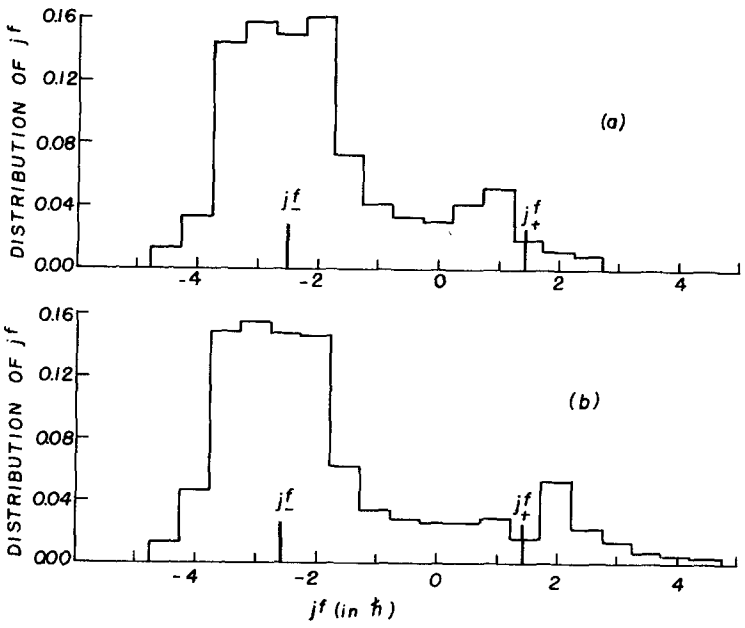

FIG. 17. Distribution of j^f for (a) $E_{tr}{}^i = 14.5$ kcal/mole, $\sigma = 0.5$ a.u., $j^i = 1.4\hbar$, $J = -2.4\hbar$; (b) $E_{tr}{}^i = 15.5$ kcal/mole, $\sigma = 0.5$ a.u., $j^i = 1.4\hbar$, $J = -2.5\hbar$.

(3) At low j^i the 2D results appear to be somewhat more statistically adiabatic than the 1 D results (Fig. 18). The one high deviation in Fig. 18 is for $j^i = \pm 5.5\hbar$, $E_{tr}{}^i = 10.55$ kcal/mole. The other high point in Fig. 19 is for $j^i = 5.5\hbar$, $E_{tr}{}^i = 14.55$ kcal/mole. The origin of their deviation is not clear to us as yet. The excess local translational energy, which is responsible for excitation of a large $\langle J_\rho \rangle$, would be expected to be less in 2D than in 1D because of other energy sinks in the 2D case. The $E_{tr}{}^{eff}$ in Fig. 19 takes cognizance of this situation.

Several notes and observations on the rotational distributions and on related topics are the following[16]:

(1) We recall first that the $j_+{}^f$ in Figs. 7–17 is b independent and that the $j_-{}^f$ in these figures is based on $b = 0.23$.

(2) At an $E_{tr}{}^i$ of 8 kcal/mole (Figs. 7 and 8) the $j_\pm{}^f$'s merely provide limits rather than expected averages, because of insufficient energy at this $E_{tr}{}^i$ to provide higher bending vibrational energy.[17] A similar situation occurred for stretching vibrational energy in the 1 D case.[2,18]

(3) At an $E_{tr}{}^i$ of 10.5–11.5 kcal/mole the $j_+{}^f$ solution is largely absent[16] except at low j^i (Fig. 12). Systems of low j^i are more easily deflected from a simple BC rotation and, perhaps, are therefore more apt to undergo the behavior in Fig. 1(a) than systems of high j^i.

(4) At an $E_{tr}{}^i$ of 14.5–15.5 kcal/mole the $j_+{}^f$ is again largely absent.

(5) At low $E_{tr}{}^i$ and $j_\pm{}^f$ describe well the adiabatic limits, while at higher $E_{tr}{}^i$ the $j_-{}^f$, with the cited b, agrees with the center of the j^f distribution. The disappearance of the $j_+{}^f$ solution has a reasonable explanation described earlier.

(6) The plot of $\gamma(s)$ in Figs. 20 and 21 for an $E_{tr}{}^i$ of 10.55 kcal/mole shows that only one of the trajectories underwent a reversal of angular motion of the type

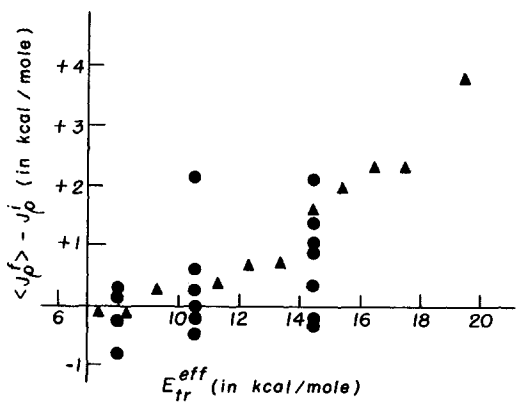

FIG. 18. Plot of $\langle J_\rho{}^f \rangle - J_\rho{}^i$ (in kilocalories/mole) versus $E_{tr}{}^i$ (in kilocalories/mole) in comparison with one- and two-dimensional results: one dimension (▲) and two dimension (●).

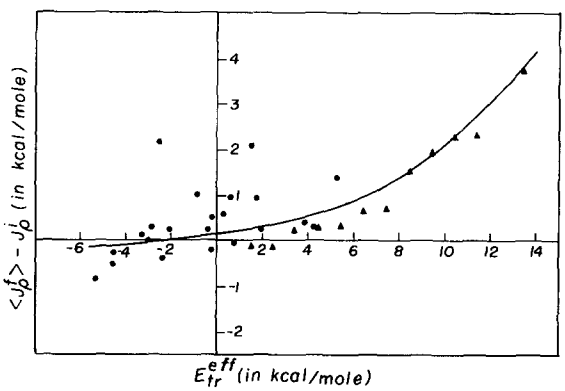

FIG. 19. Plot of $\langle J_\rho{}^f \rangle - J_\rho{}^i$ (in kilocalories/mole) versus $E_{tr}{}^{eff}$ (in kilocalories/mole) in comparison with one- and two-dimensional results: one dimension (▲) and two dimension (●).

indicated in Fig. 1(a), i.e., leading to $j_+{}^f$. The remaining five underwent the behavior of the type indicated in Fig. 1(b), i.e., leading to $j_-{}^f$. The various vibrational phases, 1–6, indicated in Figs. 20 and 21 are indicated in a plot of j^f vs vibrational phase (Fig. 22), for various rotational phases. The connection between the reversal of the γ motion (Curve 1, Fig. 20) and $j_+{}^f$ solution (which corresponds to positive j^f in the present case) is evident on comparison with Fig. 21. These results support the present interpretation of the final rotational state distribution.

(7) There is good agreement in Fig. 22 between the data calculated using natural collision coordinates and Cartesian coordinates. This fact is most encouraging, because of the extra complexities associated with dynamics of reactions in 2 D or 3 D.

(8) The range of reactive initial rotational phase

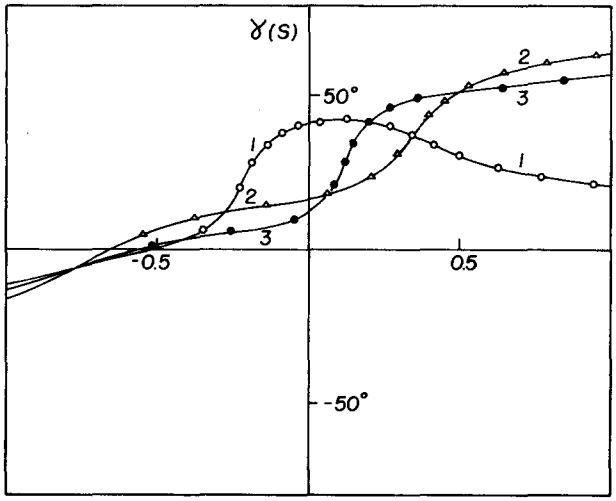

FIG. 20. Plot of γ versus s for $E_{tr}{}^i=10.55$ kcal/mole, $\sigma=0.5$ a.u., $j^i=3.5\hbar$, $\Phi=60°$, with the vibrational phases being those labeled 1, 2, 3 in Fig. 22.

$\Delta\Phi_{act}$, according to the results in Table I, is not particularly sensitive to j^i, particularly at the higher $E_{tr}{}^i$. An analogous effect was observed by Karplus, Porter and Sharma[13] in their 3 D calculations, in that their reaction cross section vs $E_{tr}{}^i$ curves were not sensitive to j^i, outside of the threshold region.

(9) The distribution of ABC (or ACB) bond angle, having a mean value of 155°, with a width of about 20° for the range of $E_{tr}{}^i$ investigated shows the extent of near-linearity of the collisions in the activated complex region.

(10) The range of reactive rotational phases $\Delta\Phi_{act}$ summarized in Table I for the conditions investigated for Reaction (1.1) is seen to vary from about 50° at an $E_{tr}{}^i$ of 8.0 kcal/mole to about 100° of an $E_{tr}{}^i$ of 14.5 kcal/mole.

One of the postulates, employed in a recent quantitative "statistical-dynamical" theory of reaction cross

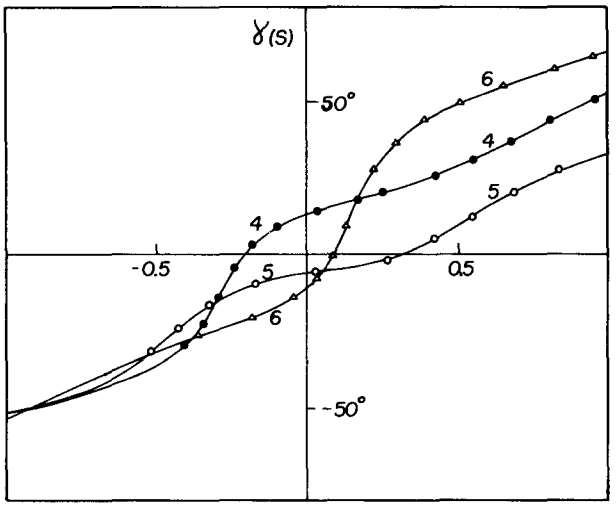

FIG. 21. Plot of γ versus s for $E_{tr}{}^i=10.55$ kcal/mole, $\sigma=0.5$ a.u., $j^i=3.5\hbar$, $\Phi=20°$, with the vibrational phases being those labeled 4, 5, 6 in Fig. 22.

sections[19] and applied, with encouraging agreement, to the $H+H_2\rightarrow H_2+H$ reaction,[20] was that the excess $E_{tr}{}^i$ increased the reaction probability by contributing toward the energy required for going from rotation of BC to bending vibration of ABC in Reaction (1.1) statistically adiabatically. The increase of $\Delta\Phi_{act}$ with

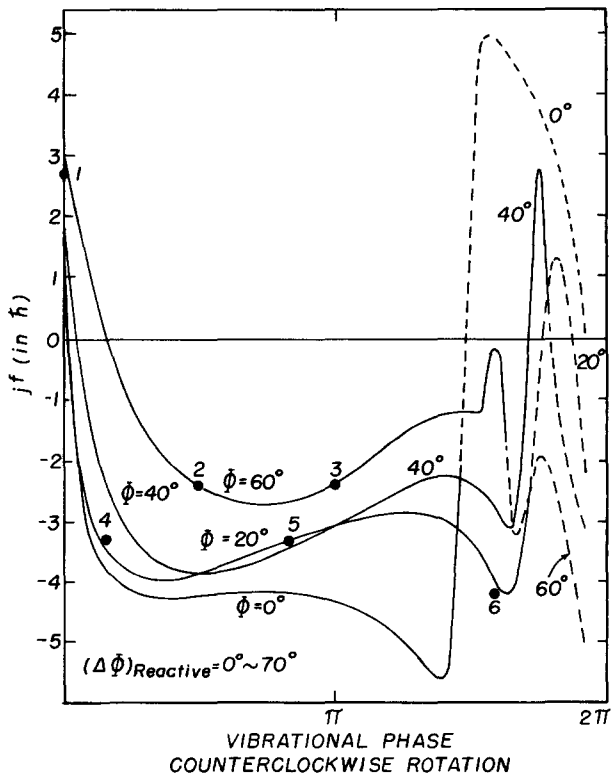

FIG. 22. Plot of j^f versus vibrational phase for $E_{tr}{}^i=10.55$ kcal/mole, $\sigma=0.5$ a.u., $j^i=3.5\hbar$ and various Φ's. The circle points (●) are those obtained using natural collision coordinates.

E_{tr}^i and the near-adiabaticity of J_ρ are consistent with the postulates.

The results on dependence of J_ρ^f and j^f on both the initial rotational and vibrational phase indicate a significant rotational–vibrational coupling. The treatment in Paper IV can be modified to allow for a particular coupling in zeroth order, by solving first for the adiabatic vibrational solution, treating the angle variable γ, like s, as a slowly varying parameter. The correlations embodied in Eqs. (2.2) and (2.3)–(2.10) would not be affected, but the *ab initio* calculation of b would be modified, to allow for a dependence of the local ρ-vibrational energy on both γ and s. (In Paper IV it depended only on s.)

APPENDIX A: COORDINATES AND PHASES FOR EXACT CALCULATION

The Cartesian coordinates of B relative to those of C are (Q_1, Q_2); those of A relative to the same center are (Q_3, Q_4). The conjugate momenta are $P_1, \cdots, P_4$. In terms of the impact parameter σ, the initial relative velocity V_R, a reaction-shell distance q_0 where the interaction of A and BC is negligible, the initial orientation of BC Φ, and the initial length of BC distance r^i, the initial values used for Q_1, Q_2, Q_3, Q_4, P_1, P_2, P_3, P_4 are $r^i\cos\Phi$, $r^i\sin\Phi$, $-(q_0^2-\sigma^2)^{1/2}$, σ, $-(j^i/r^i)\sin\Phi+p_r{}^i\cos\Phi$, $(j^i/r^i)\cos\Phi+p_r{}^i\sin\Phi$, $\mu_{A,BC}V_R$, 0, where $\mu_{A,BC}=m_A(m_B+m_C)/(m_A+m_B+m_C)$ and p_r is the momentum conjugate to r, initially equal to $p_r{}^i$.

The initial vibration action j_ρ is computed from the standard formula $\oint p_r dr$, noting that

$$p_r{}^2/2\mu_{BC}=E-E_{tr}{}^i-(j^{i2}/8\pi^2\mu_{BC}r^2)-V(r), \quad \text{(A1)}$$

where $V(r)$ is the vibrational potential energy. The vibrational and rotational energies of the isolated molecule BC are not exactly constants, but J_ρ and j^i are.

The Φ was chosen uniformly. The initial vibrational phase δ was chosen uniformly by selecting uniformly spaced initial times in the initial vibrational motion,[21] at constant initial separation distance between A and BC, i.e., constant $(Q_3^2+Q_4^2)^{1/2}$. Hamilton's equations were then integrated numerically using Cartesian coordinates, and the final values of the latter were subsequently transformed to j^f, $J_\rho{}^f$, etc., using equations paralleling those above.

APPENDIX B: *AB INITIO* CALCULATION OF THE PARAMETER b AND OF $\gamma(s)$

For completeness we summarize here the relevant equations of Paper IV needed for the *ab initio* calculation of b.

Equation (61) there, when one substitutes the relation

$$J_\gamma{}^I=2\pi\,|\,-j^i+bJ\,|, \quad \text{(B1)}$$

becomes

$$2\pi\,|\,-j^i+bJ\,|/(32IA)^{1/2}=(k_1{}^2-1)K(k_1)+E(k_1), \quad \text{(B2)}$$

where the notation is the same as in Part IV.

Equation (20) there reads

$$b=|\,F(s)r_0{}^2(s)/R_0{}^2(s)\,|, \quad \text{(B3)}$$

where these quantities are defined in Part IV. Iteration of (B2) and (B3) yields an *ab initio* value for b. The latter is found to be 0.10 a.u. for $j^i=1.4\hbar$ and 0.14 a.u. for $j^i=\pm5.5\hbar$ and $\pm3.3\hbar$. As noted in the text the strong rotational-vibrational coupling will modify the effective energy available to the γ motion, and so modify this numerical value of this *ab initio* b. The empirical value for b in the text is 0.23 a.u.

To calculate the $\gamma(s)$ given in Figs. 20 and 21 it was necessary to integrate the equations of motion in natural collision coordinates, obtained from the Hamiltonian H given by Eqs. (27) and (28) in Part III, where one may set $\dot r_0=0$ and $A_m=0$. [A_m is zero if one chooses function $\zeta(s)$ according to Eq. (13) in Part III.]

$$H=(2\mu)^{-1}\left\{\frac{p_s{}^2}{\eta^2}+p_\rho{}^2+\frac{p_\gamma{}^2}{r^2}+\frac{[p_\varphi\mp Fp_\gamma+(A_{sp}p_s/\eta)]^2}{[R^2-A_{sp}{}^2-r^2F^2]}\right\}+V(s,\rho,\gamma), \quad \text{(B4)}$$

where $A_{sp}=A_s r\sin\gamma/\eta$ and the notation of Papers III and IV is used.

The upper sign is used for positive z branch (i.e., Curve C in Fig. 7 of Paper III, the reaction path for A+BC→AB+C), while the lower sign is used for negative z branch (i.e., Curve G, the reaction path for A+BC→AC+B). The appropriate functions for two branches of coordinate z should be used.[2,4,5] Treating $(s, \rho, \gamma, \varphi)$ as independent variables one obtains the Hamilton's equations of motion from (B4) in the standard way.

Some care is needed in transforming (when necessary) from positive z branch to negative z branch of the reaction coordinate, and vice versa, to allow the two possible channels, A+BC→AB+C and A+BC→AC+

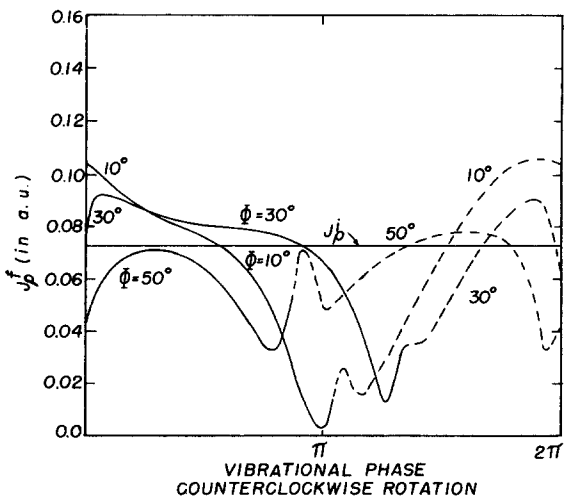

FIG. 23. Plot of $J_\rho{}^f$ versus vibrational phase for $E_{tr}{}^i=8.0$ kcal/mole, $\sigma=0.25$ a.u., $j^i=3.5\hbar$ and various Φ's.

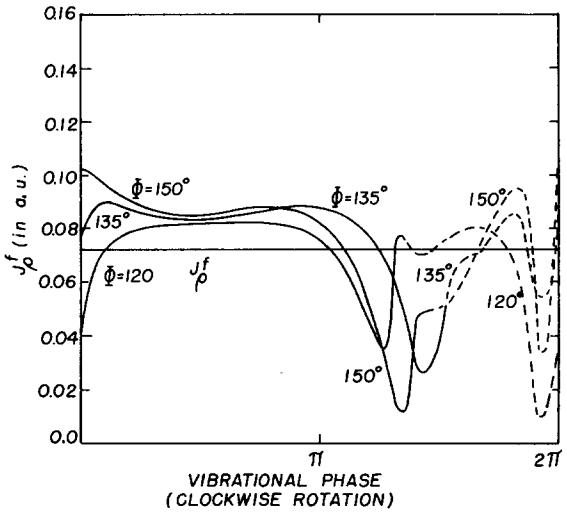

FIG. 24. Plot of $J_\rho{}^f$ versus vibrational phase for $E_{tr}{}^i=8.0$ kcal/mole, $\sigma=0.25$ a.u., $J^i=-3.5\hbar$ and various Φ's.

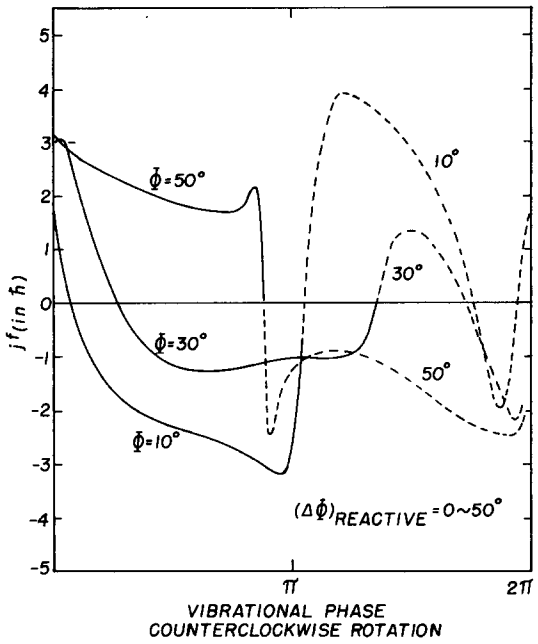

FIG. 26. Plot of j^f versus vibrational phase for $E_{tr}{}^i=10.55$ kcal/mole, $\sigma=0.5$ a.u., $j^i=-3.5\hbar$ and various Φ's.

B, to occur. In the cylindrically symmetric region of the reaction path, Curve C or Curve G, the transformation is accomplished merely by noting that if γ is in the interval $[-\pi/2, \pi/2]$, the system is in positive z branch; if it is in the interval $[\pi/2, 3\pi/2]$, the system is in negative z branch. When the reaction path (Curve C or G) begins to bend one should define the branch in terms of its value of z (i.e., whether it is positive or negative) rather than its value of γ. Because the natural collision coordinates $(s, \rho, \gamma, \varphi)$ have the same value for two branches at the $z=0$ plane, the coordinate transformation from Cartesian coordinates to $(s, \rho, \gamma, \varphi)$ can be used to transform the momenta in one z branch into those in space-fixed coordinate system, and then the latter momenta can be transferred back to the natural collision coordinate system in the other z branch.

APPENDIX C: DEPENDENCE OF J_ρ AND j^f ON VIBRATIONAL AND ROTATIONAL PHASE

Representative data used in building up Table I and the previous figures in this paper are given in Figs. 23–25 for $J_\rho{}^f$ and in Figs. 26 and 27 for j^f (as well as Fig. 22). All these figures indicate effects of vibrational–rotational coupling. In the $J_\rho{}^f$ plots there is some indication of an "isobestic-type" behavior, the curves

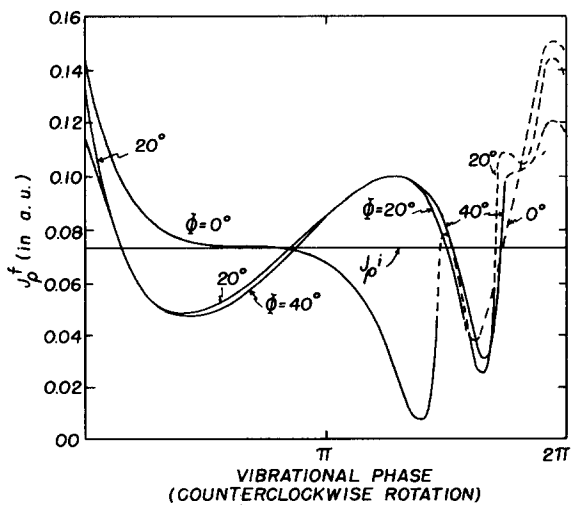

FIG. 25. Plot of $J_\rho{}^f$ versus vibrational phase for $E_{tr}{}^i=10.55$ kcal/mole, $\sigma=0.5$ a.u., $J^i=3.5\hbar$ and various Φ's.

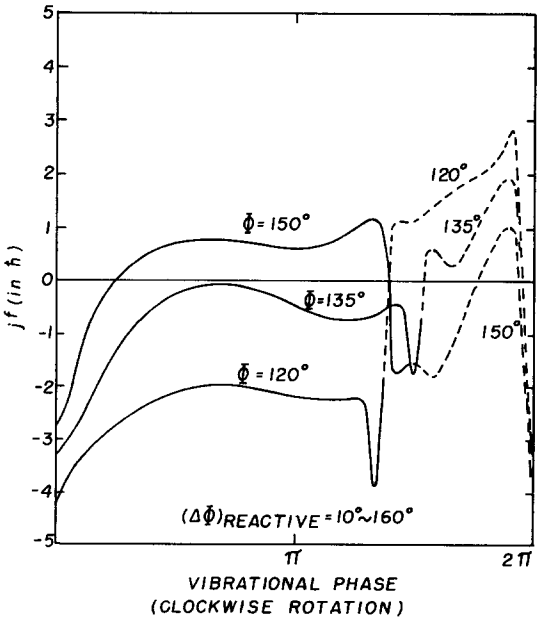

FIG. 27. Plot of j^f versus vibrational phase for $E_{tr}{}^i=8.0$ kcal/mole, $\sigma=0.25$ a.u., $j^i=-3.5\hbar$, and various Φ's.

for various Φ's tending to oscillate about the curve for some particular Φ. The j^f plots are more sensitive to Φ than are the $J_p{}^f$ plots. Similar behaviors are also observed for other initial conditions given in Table I.

The several j^f plots at a given positive j^i and at various $E_{tr}{}^i$'s are found to be all of a similar shape (e.g., Fig. 22). Similar remarks apply for negative j^i.

* Acknowledgement is made to the National Science Foundation and to the donors of the Petroleum Research Fund, administered by the American Chemical Society, for their support of this research.

[1] R. A. Marcus, J. Chem. Phys. **43,** 1598 (1965).

[2] R. A. Marcus, J. Chem. Phys. **45,** 4493, 4500 (1966), Papers I and II.

[3] R. A. Marcus, Discussions Faraday Soc. **44,** 7 (1967).

[4] R. A. Marcus, J. Chem. Phys. **49,** 2610 (1968), Paper III.

[5] R. A. Marcus, J. Chem. Phys **49,** 2617 (1968), Paper IV.

[6] S. F. Wu and R. A. Marcus, J. Chem. Phys. **53,** 4026 (1970), Paper V.

[7] J. O. Hirschfelder and E. Wigner, J. Chem. Phys. **7,** 616 (1939); M. A. Eliason and J. O. Hirschfelder, *ibid.* **30,** 1426 (1959); L. Hofacker, Z. Naturforsch. **18A,** 607 (1963); R. A. Marcus, J. Chem. Phys. **46,** 959 (1967), and Ref. 1. For recent interesting discussions see also D. G. Truhlar, *ibid.* **53,** 2041 (1970); D. G. Truhlar and A. Kupperman, *ibid.* **53,** 3841 (1970); K. Morokuma and M. Karplus *ibid.* **51,** 5193 (1969).

[8] M. S. Child, Discussions Faraday Soc. **44,** 69 (1967).

[9] For example, statistical adiabaticity from products to activated complex ensures that activated complex theory is obeyed for the reverse step and hence, by microscopic reversibility, for the forward step.

[10] The first, second, and third terms on the right side of Eq. (14) of Ref. 6 [or of Eq. 93 of Ref. 5] represent adiabatic, statistical adiabatic, and nonadiabatic terms, respectively. The fourth term there, Δ, is a statistical adiabatic one.

[11] R. A. Marcus (unpublished).

[12] The step size of integration, Δt, was 0.02×10^{-14} sec, which is approximately 1/25 of the vibrational period of H_2 molecule, and the radius of reaction shell, q_0, was set at 8.0 a.u.

[13] R. N. Porter and M. Karplus, J. Chem. Phys. **40,** 1105 (1964).

[14] M. Karplus, R. N. Porter, and R. D. Sharma, J. Chem. Phys. **43,** 3259 (1965); **40,** 2033 (1964).

[15] The anharmonicity correction, not noted in (3.3), for the bending vibrational energy term was negligible for the present conditions. Some of the numerical values used for terms in (3.3) are as follows: $E_{vib}{}^l$ is $J_\gamma{}^l\nu_\gamma{}^\ddagger$ a.u. (1 a.u. equals 627.23 kcal/mole), $\nu_\gamma{}^\ddagger$ was calculated from the data in Ref. 13: $\nu_\gamma{}^\ddagger$ equals $(2\pi)^{-1}\times(A_{22}/\mu)^{1/2}$, where $(A_{22}/\mu)^{1/2}$ equals $[0.0244/(\frac{2}{3}\times1.0079)]^{1/2}=0.19056$ a.u. The other properties of this potential energy surface in Refs. 13 and 14 are as follows: zero-point energy of symmetric stretching and of each bending vibration is 3.12 and 1.40 kcal/mole. The potential energy at the saddlepoint is 9.13 kcal/mole. Thus, the adiabatic threshold energy $E_{ad}{}^0$ for the one-dimensional case, for lowest vibrational state, is 12.25 kcal/mole, and for the 2-D case it is $12.25+J_\gamma{}^l\nu_\gamma{}^\ddagger+J^2\hbar^2/2\mu R^{\ddagger 2}$.

[16] Only the substantial wide peaks in Figs. 2–17 are significant. Occasional narrow *isolated* peaks, as in Fig. 9(a) at $j^f=-5\hbar$ and Fig. 11(b) at $j^f=-3.5\hbar$, are probably spurious, reflecting the limited data.

[17] All j^f's lying outside this interval have a lower $J_\gamma{}^l$.

[18] Compare with R. A. Marcus, Discussions Faraday Soc. **44,** 87 (1967), based on results of M. Karplus and K. Morokuma, *ibid*, p. 78.

[19] R. A. Marus, J. Chem. Phys. **45,** 2630 (1966).

[20] R. A. Marcus, J. Chem. Phys. **46,** 959 (1967).

[21] The same procedure was used in Ref. 14, with minor differences.

THE JOURNAL OF CHEMICAL PHYSICS VOLUME 56, NUMBER 7 1 APRIL 1972

Theoretical Study of the F_2 Molecule Using the Method of Optimized Valence Configurations

G. DAS AND ARNOLD C. WAHL

Chemistry Division, Argonne National Laboratory, Argonne, Illinois 60439

(Received 5 October 1971)

The method of optimized valence configurations (OVC) is used to study the potential curve for the ground state of the F_2 molecule. All the important electron correlation-effects within and between various molecular shells are investigated via the multiconfiguration self consistent field (MCSCF) process. It is found that, consistent with the philosophy of the OVC method, these effects fall into two distinct categories: (1) the molecular correlation, which vanishes when the molecule dissociates into the constituent atoms, and (2) the atomic correlation, which passes asymptotically to that for the atoms. The very weak interdependence or "coupling" of the two correlation types results in considerable computational simplification by permitting MCSCF calculations to be performed on groups, consisting of a comparatively small number of configurations, and the evaluation of their respective contributions to the bonding interaction by a simple summation in the spirit of pair theory. Such calculations on F_2 yield a potential curve which is very similar to the one derived from experiment. Our calculated values of the spectroscopic constants D_e, ω_e, R_e are, respectively, 1.67 eV, 942 cm^{-1}, 2.67 bohr. These are in good agreement with the corresponding experimental values 1.68 eV, 932 cm^{-1}, 2.68 bohr. General rules are given for applying this procedure to other molecular systems.

I. INTRODUCTION

The quantitative description of the ground state of the F_2 molecule has presented a challenge to the discipline of theoretical chemistry for several generations. Theoretical interest in this molecule can be traced to its anomalous properties and the fact that its valence bond wavefunction is rather simple.[1] There exists in the literature configuration interaction (CI) calculations of various types including valence bond,[2,3] the "atoms in molecule approach",[4] minimal basis set SCF,[5] and extended basis set SCF studies of near